

# MAGNETOSPHERIC MULTISCALE (MMS) MISSION ATTITUDE GROUND SYSTEM DESIGN

**Joseph E. Sedlak,<sup>(1)</sup> Emil A. Superfin,<sup>(2)</sup> and Juan C. Raymond<sup>(3)</sup>**

<sup>(1)</sup>*a.i. solutions, Inc., 10001 Derekwood Lane, Lanham, MD 20706, USA, joseph.sedlak@ai-solutions.com*

<sup>(2)</sup>*a.i. solutions, Inc., 10001 Derekwood Lane, Lanham, MD 20706, USA, emil.superfin@ai-solutions.com*

<sup>(3)</sup>*NASA/Goddard Space Flight Center, Code 591, Greenbelt, MD 20771, USA, juan.c.raymond@nasa.gov*

**Abstract:** This paper presents an overview of the attitude ground system (AGS) currently under development for the Magnetospheric Multiscale (MMS) mission. The primary responsibilities for the MMS AGS are definitive attitude determination, validation of the onboard attitude filter, and computation of certain parameters needed to improve maneuver performance. For these purposes, the ground support utilities include attitude and rate estimation for validation of the onboard estimates, sensor calibration, inertia tensor calibration, accelerometer bias estimation, center of mass estimation, and production of a definitive attitude history for use by the science teams. Much of the AGS functionality already exists in utilities used at NASA's Goddard Space Flight Center with support heritage from many missions, but new utilities are being created specifically for the MMS mission, such as for the inertia tensor, accelerometer bias, and center of mass estimation. Algorithms and test results for all the major AGS subsystems are presented here.

**Keywords:** MMS, attitude, ground support

## 1. Introduction

This paper describes the attitude ground system (AGS) design to be used for support of the Magnetospheric MultiScale (MMS) mission. The AGS exists as one component of the mission operations control center. It has responsibility for validating the onboard attitude and accelerometer bias estimates, calibrating the attitude sensors and the spacecraft inertia tensor, and generating a definitive attitude history for use by the science teams.

NASA's Goddard Space Flight Center (GSFC) in Greenbelt, Maryland is responsible for developing the MMS spacecraft, for the overall management of the MMS mission, and for mission operations. MMS is scheduled for launch in 2014 for a planned two-year mission.

The MMS mission consists of four identical spacecraft flying in a tetrahedral formation in an eccentric Earth orbit. The relatively tight formation, with separations ranging from 10 to 400 km, will provide coordinated observations giving insight into small-scale magnetic field reconnection processes. By varying the size of the tetrahedron and the orbital semi-major axis and eccentricity, and making use of the changing solar phase, this geometry allows for the study of both bow shock and magnetotail plasma physics, including acceleration, reconnection, and turbulence. The mission divides into two phases for science; these phases will have orbit dimensions of  $1.2 \times 12$  Earth radii in the first phase and  $1.2 \times 25$  Earth radii in the second in order to study the dayside magnetopause and the nightside magnetotail, respectively. The orbital periods are roughly one day and three days for the two mission phases.

Each of the four MMS spacecraft will be spin stabilized at 3 revolutions per minute (rpm), with the spin axis oriented near the ecliptic north pole but tipped approximately 2.5 deg towards the Sun line. The main body of each spacecraft is an eight-sided platform with diameter of 3.4 m and height of 1.2 m. Several booms are attached to this central core: two axial booms of 14.9 m length, two radial magnetometer booms of 5 m length, and four radial wire booms of 60 m length. Attitude and orbit control will use a set of axial and radial thrusters. A four-head star tracker (ST) and a slit-type digital Sun sensor (DSS) provide input for attitude determination. In addition, an accelerometer will be used for closed-loop orbit maneuver control.

---

This work was supported by the National Aeronautics and Space Administration (NASA)/Goddard Space Flight Center (GSFC), Greenbelt, MD, USA, Contract NNG10CP02C.

22<sup>nd</sup> International Symposium on Spaceflight Dynamics, INPE, São José dos Campos, SP, Brazil, February 2011.

The primary AGS product will be a daily definitive attitude history. An extended Kalman filter (EKF) will be used to estimate the three-axis attitude (both the spin axis orientation and spin phase) and the rotation rate for all times when the tracker data is available. If there are gaps in the ST data, these will be interpolated, as described in Sec. 2.1, to create the definitive attitude product.

The four ST heads have separate fields of view that must be calibrated on-orbit to correct for launch shift. Section 2.2 describes the alignment calibration for both the ST and the DSS.

To improve the accuracy of the closed-loop orbit maneuver control, the accelerometer bias must be estimated whenever a burn is planned. Section 2.3 presents the bias estimation algorithm and describes some test cases.

The current MMS spacecraft design does not include rate-sensing gyroscopes, so the EKF must use dynamical modeling for attitude and rate propagation. One consequence of this is that the accuracy of the transverse components of the estimated rotation rate is very sensitive to errors in the inertia tensor. The computed centripetal accelerations are affected by these rate errors; thus, the accelerometer bias estimation accuracy is affected by the inertia tensor accuracy. Section 2.4 gives a detailed description of the AGS approach to improving the inertia tensor knowledge on-orbit.

Maneuvers on thrusters will impart unintended angular momentum to the spacecraft in proportion to the error in the moment arm of the thrust relative to the center of mass (CM). To reduce the error in the CM knowledge, the AGS will attempt to estimate the CM position using the Doppler shifts of Global Positioning System (GPS) carrier frequencies. Section 2.5 shows a derivation of the required partial derivatives and gives some very preliminary results.

Concluding remarks are given in Sec. 3.

## 2. AGS Utilities

This section describes the AGS subsystems needed for MMS support. These include attitude estimation, validation of the onboard attitude, sensor interference prediction, and several types of calibration described below. In addition, the AGS has many other features that include capabilities such as:

- Estimating the attitude by a variety of methods (extended Kalman filter, optimal smoother, or single-frame quaternion estimation (QUEST) [1])
- Generating reference vectors (Sun, Earth, Moon, magnetic field, and guide stars) in the body frame, the geocentric inertial (GCI) frame, or other special-purpose frames
- Plotting and flagging measurement vectors, attitude solutions, and sensor residuals
- Generating time-dependent visualizations of sensor fields of view (FOV) including stars to magnitude 9, Sun, Earth, Moon, and planets
- Identifying tracked stars

This wide variety of features puts the AGS at the heart of a powerful ground support system that has proven invaluable on over two dozen missions for nominal support, calibrations, data analysis, and anomaly resolution.

The AGS was initially created as a general system for three-axis stabilized spacecraft mission support [2] and has grown, as needed, by adding capabilities to satisfy specific mission requirements, including some features for spin-stabilized spacecraft support. The MMS spacecraft are spinners. However, they carry autonomous quaternion-output star trackers, and the attitude products require full three-axis attitudes (not just the spin axis direction). For these reasons, the ground system is well served by using a three-axis support system rather than one designed just for spin-stabilized spacecraft. The oldest parts of the AGS were written in FORTRAN in the 1970s and 1980s. The generalized multimission version [2] was created in the early 1990s and was used to support, e.g., the UARS, EUVE, and RXTE missions. The AGS was ported to MATLAB in the late 1990s.

## 2.1. Attitude Sensors and Attitude Products

**2.1.1. Attitude Sensors.** The MMS spacecraft sensor complement consists of a star tracker (ST) with four separate heads and two redundant digital Sun sensors (DSS) (one being a cold back-up unit). The four ST heads output four independent quaternions at 4 Hz (that is, 16 independent attitude measurements per second). However, the AGS probably will be using telemetry with only a 1 Hz data rate (4 attitudes per second). Once per spin period ( $\sim 20$  sec), the DSS will output a pulse indicating sun-crossing through the sensor FOV slit and a measurement of the Sun elevation from the body X-Y-plane (the +Z-axis is the nominal spin axis).

All four ST heads are aligned roughly 10 deg offset from the body -Z-axis and are mounted two each on two separate stable optical benches. This orientation is a compromise between minimizing the star motion through the FOVs and avoiding interference from an axial sensor boom deployed along the -Z-axis direction. An alignment transformation is applied to the output from each ST head so the final output quaternions all represent transformations from the GCI frame to the body frame.

In addition, there is an acceleration measurement system (AMS) comprising two redundant sets of three orthogonal accelerometers. The AMS is used primarily as part of the closed-loop delta-V maneuver control system but also can be used in the attitude filter. The centripetal acceleration is proportional to the square of the rotation rate and provides a measure of two components of the rate. The AMS is mounted approximately 0.37 m radially from the spin axis.

**2.1.2. Definitive Attitude Products.** The AGS currently plans to deliver a definitive attitude product for every orbit of the mission, perigee-to-perigee, after commissioning. The attitude accuracy requirement is 0.1 deg ( $3\sigma$ ) per axis for all regions of interest (ROI) to the science team, and best available outside of the ROI. (The ROI usually are near apogee or near perigee, depending on mission phase.)

It is now expected that ST data will be available for all ROI. However, earlier in the mission planning, there were power concerns indicating that the ST could only be powered on for perhaps 10 percent of each orbit. That led to an AGS design that allowed for partial data coverage.

For all time spans with valid ST data, the AGS will generate attitude and rate solutions using an EKF, discussed below. If there are gaps in the data, these will be bridged by assuming the angular momentum is constant in both the GCI and body frames. The resulting attitude history is the definitive attitude. When filling any data gaps, the major principal axis of inertia is aligned with the angular momentum direction (e.g., the mean angular momentum estimated from the data sets before and after the gap). The spin phase in the gaps is computed using the DSS Sun pulses to maintain synchronization. If there also is a gap in DSS data due to eclipse, the spin phase will be interpolated using a constant rate from the last DSS Sun pulse of one data set to the first Sun pulse of the next data set, or extrapolated using the mean rate determined by the EKF.

With this approach, the resulting attitude solutions in the data gaps do account for coning (misalignment of the major principal axis from the body Z-axis), but not for nutation (offset of the angular momentum vector in the body frame from the major principal axis). Any nutation is expected to be damped to an amplitude less than 0.1 deg, except possibly for orbits immediately following maneuvers, so this is not a concern.

**2.1.2.1. Kalman Filter.** The spinning spacecraft EKF used in the AGS, referred to here as SpinKF, is the SpinKF-I described in [3]. The original SpinKF implementation is given in [4]. SpinKF is conceptually similar to the “standard” Lefferts, Markley, and Shuster quaternion and rate filter described in [5]; however, the SpinKF state vector avoids using the quaternion. Instead, the SpinKF uses a seven-parameter angular-momentum-based representation [6]. The seven elements of the state vector are the three angular momentum components in the GCI frame, the three angular momentum components in the spacecraft’s body frame, and a spin phase angle. These parameters

are subject to the constraint that the magnitude of the angular momentum is the same in the inertial and body frames (just as the standard quaternion and rate filter has seven state components with the constraint that the quaternion be normalized).

The value of the angular-momentum-based representation is improved numerical accuracy. Most spinning spacecraft do not carry rate-sensing gyros; thus, the Kalman filter for a spinner usually must integrate the dynamics equations to propagate the state between observations. This numerical integration is more accurate for a set of parameters having less variation. For spinning spacecraft, all four quaternion components are rapidly varying. The angular-momentum-based representation has only a single rapidly varying component; that is the spin phase, and it is increasing only linearly (modulo  $2\pi$ ) rather than varying sinusoidally.

The SpinKF algorithm has been used operationally for the ST-5 and THEMIS missions. It has been tested for MMS with several scenarios using a simple simulator and also with a high-fidelity simulation including oscillations of the flexible wire booms and other appendages. The attitude estimation error has been found to be well under the required 0.1 deg ( $3\sigma$ ) tolerance. Typical  $3\sigma$  errors are roughly 0.05 deg about the Z-axis and 0.02 deg about X and Y.

**2.1.2.2. Attitude Validation.** To validate the performance of the onboard EKF, the onboard attitude estimates will be compared with the SpinKF attitudes for a time span of roughly two hours each day (the actual time span is yet to be negotiated). The mean and standard deviation of these attitude residuals will be reported to the mission operations center (MOC).

In addition, SpinKF statistics for the attitude, rate, and individual sensor residuals will be saved in a trending database. This database serves two important purposes: it allows the AGS team to spot early signs of sensor degradation, and it shows how fast the angular momentum is precessing in the GCI frame due to environmental torques.

**2.1.3. Predicted Attitude Products.** Using the most recent definitive attitude product for initialization, an attitude prediction will be generated periodically. Early in the mission, this prediction will be created by assuming the major principal axis of inertia is aligned with the angular momentum vector, which is assumed constant in GCI. As trending data accumulates, it may prove useful to include a simple empirical model of the daily spin axis drift. This drift is caused by a combination of gravity gradient, drag, and solar pressure torques, but these torques will not be modeled explicitly. It is expected that the drift will be less than 0.01 degrees per day.

The predicted attitude will be used for two purposes. First, it will indicate when the next attitude maneuver is needed to maintain the correct spin axis orientation with respect to the Sun and ecliptic pole. This maneuver will be scheduled roughly every two weeks. Second, the predictions will be used to indicate when to expect Earth or Moon interference in the ST or DSS. Since the spin phase cannot be predicted, the interference report will not tell which ST head is occulted versus time, but it will indicate the fraction of each spin period subject to interference for each head.

## 2.2. Attitude Sensor Alignment Calibration

Early in the commissioning phase of the MMS mission, the ST and DSS will be calibrated for alignment. It is possible that the seasonal variation of the solar beta angle will cause thermal variations that affect the alignments. If these prove to be significant, then the alignment calibrations may be repeated, as needed. It must be emphasized that in-flight calibration can only correct for relative misalignment and not for absolute alignments in the body frame. In effect, the mean alignment of the four ST heads defines the body frame on orbit.

**2.2.1. ST Alignment Calibration.** The four ST heads are located pair-wise on two optical benches. Their prelaunch alignments will be measured by optical methods using reflective cubes on the benches. Alignment calibration is performed on-orbit to correct for any shift due to launch shock, release of gravitational stress, and change of thermal environment.

The relative alignment of two heads on the same bench is likely to remain more stable than two heads on separate benches. (This will be monitored as trending data is collected throughout the mission.) Nonetheless, the relative alignments of all four heads will be determined after launch.

The AGS calibration utility will use the ALIQUEST method [7]. This attitude-dependent method solves for the misalignment using a reference attitude and is based on the QUEST quaternion estimation algorithm [1]. The QUEST algorithm is a well-known, efficient, and reliable method to determine the attitude by minimizing the loss function,  $L$ , as a function of the attitude matrix,  $A$ ,

$$L(A) = \sum_i [\vec{v}_i^{body} - A \vec{v}_i^{ref}]^2 , \quad (1)$$

where vector  $\vec{v}_i^{body}$  is the observation unit vector for sensor  $i$  expressed in the body frame,  $\vec{v}_i^{ref}$  is the corresponding inertial frame reference vector, and index  $i$  runs over all sensors available at a given time. The matrix  $A$  is the “single-frame” attitude estimate at that time. Similarly, the attitude-dependent alignment estimation problem can be cast in a parallel form. That is, determine the misalignment for a given sensor by minimizing the loss function

$$L(O) = \sum_j [O \vec{v}_j^{body} - A_j \vec{v}_j^{ref}]^2 \quad (2)$$

as a function of the orthogonal misalignment matrix,  $O$ , where subscript  $j$  is a time index running over all valid observations, and  $A_j$  is the known attitude history. The vector  $\vec{v}_j^{body}$  is the observation unit vector for the given sensor, rotated to the body frame using the nominal alignment,  $N_o$ , and any a priori misalignment,  $M_o$ . Once  $O$  is determined, the new misalignment is usually expressed in the sensor frame as

$$M = N_o^{-1} O N_o M_o , \quad (3)$$

where the inverse of  $N_o$  is used here rather than the matrix transpose to allow for possible nonorthogonality. It is clear Eqs. 1 and 2 can be minimized using the same method. Choosing the QUEST algorithm [1] to solve Eq. 2 results in the ALIQUEST utility. For quaternion-type trackers as on MMS, one can create effective vector measurements from the sensor boresight and an arbitrary orthogonal vector for use in Eq. 2. Alternatively, one can recast the solution as a matrix mean value that does not use the QUEST algorithm. See [7] for details.

For the MMS ST calibration, the reference attitude will be generated using approximately the same number of pre-calibration observations from each ST head, all with the same weight. This makes the reference attitude, in effect, an average over all four misalignments. After the calibration, the alignments of the four ST heads will have been adjusted to agree with this reference attitude. Thus, when the calibrated ST data is used in an attitude filter, the ST residuals will be reduced but the attitude solution should be unchanged. This means that ALIQUEST calibrations can be performed at any time during the mission without introducing any discontinuity in the definitive attitude histories being delivered daily to the science teams.

**2.2.2. DSS Alignment Calibration.** While the four ST heads provide almost all of the data needed by the SpinKF attitude filter, the DSS also contributes some attitude and rate information. The DSS contribution is much smaller than that of the ST since it is available only once per spin and its intrinsic errors are larger than those of the ST. Nonetheless, if the DSS is misaligned with respect to the ST, its use in the filter can actually make the solutions worse. Thus, it is important to calibrate the alignment of the DSS relative to the ST early in the mission.

The ST head alignment will be performed first, as described above. This assures that an ST-based attitude solution will be the best available as a reference attitude. The ALIQUEST utility will use this reference attitude to determine the mean systematic error in the DSS data.

The only difference between the DSS and ST calibrations is that the DSS alignment component about the Sun vector is not observable. The Sun vector measurement in the body frame will be nearly constant over the entire calibration data set. (It can be exactly constant if all Sun measurements fall within the same digitization bin.) This can cause the ALIQUEST alignment correction matrix to have a large error about the axis corresponding to the Sun direction [7]. To avoid this problem, the correction matrix is expressed as three Euler angles, with the third Euler axis along the Sun direction. To remove the error, the final correction matrix is composed of just the first two Euler angles, with the third angle set to zero. This is equivalent to representing the DSS correction as an azimuthal rotation of the detection slit and an elevation rotation along the direction of the slit.

### 2.3. Accelerometer Calibration

During the AGS design process, it was decided that two different accelerometer calibrations may be necessary to meet orbit maneuver requirements. The two calibration parameters are bias and scale factor. At the time of this paper's writing, only bias estimation has been prototyped and tested. The actual need for scale factor calibration is still under study.

The accelerometer is used for onboard, closed-loop, delta-V maneuver control. There will be an onboard accelerometer bias estimator. The AGS will use an independent method to validate the onboard estimates. The required accuracy for maneuver support is  $2 \mu\text{g}$  ( $3\sigma$ ) per axis.

The AGS filter for the accelerometer bias works in conjunction with the attitude and rate filter. This combination is a type of “cascaded” filter. This name comes from the way in which both filters run simultaneously, but information flows only in one direction – from the attitude and rate filter to the bias filter.

The bias filter is designed as a standard EKF with a 3-element state vector representing the accelerometer bias for each axis. The measurement residual is

$$\vec{r}_{acc} = \vec{a}_{obs} - \vec{a}_{est}, \quad (4)$$

where  $\vec{a}_{obs}$  is the accelerometer observation, and where the estimated measurement is

$$\vec{a}_{est} = \frac{d\vec{\omega}}{dt} \times \vec{R}_{acc} + \vec{\omega}_i \times (\vec{\omega}_i \times \vec{R}_{acc}) + \vec{b}_i(-), \quad (5)$$

using the dynamics equation

$$\frac{d\vec{\omega}}{dt} = J^{-1}(\vec{L}_B \times \vec{\omega}_i + \vec{T}), \quad (6)$$

and where the angular momentum in the body frame is

$$\vec{L}_B = J\vec{\omega}_i. \quad (7)$$

The vector  $\vec{R}_{acc}$  runs from the center of mass to the accelerometer and is given in meters,  $\vec{\omega}_i$  is the rate estimate in rad/sec taken from the attitude and rate filter at time  $t_i$ ,  $\vec{b}_i(-)$  is the a priori bias estimate in m/sec<sup>2</sup> at time  $t_i$ , and  $\vec{T}$  is the torque expressed in the body frame, which could be calculated from thruster data (however this bias filter is not expected to be run during the actual burns, so  $\vec{T}$  will generally be zero).

The partial derivative of the observation model given by Eq. 5 with respect to the bias estimate yields the sensitivity matrix needed by the EKF,

$$H = I_3, \quad (8)$$

where  $I_3$  is the 3×3 identity matrix.

The bias filter was tested first using a set of rigid body simulation data. The results of a sample run are shown in Fig. 1. It was found in all such tests that the filter could predict the bias to within  $0.9 \mu\text{g}$  ( $3\sigma$ ) per axis, with a run time of four hours and observations at 4 Hz.

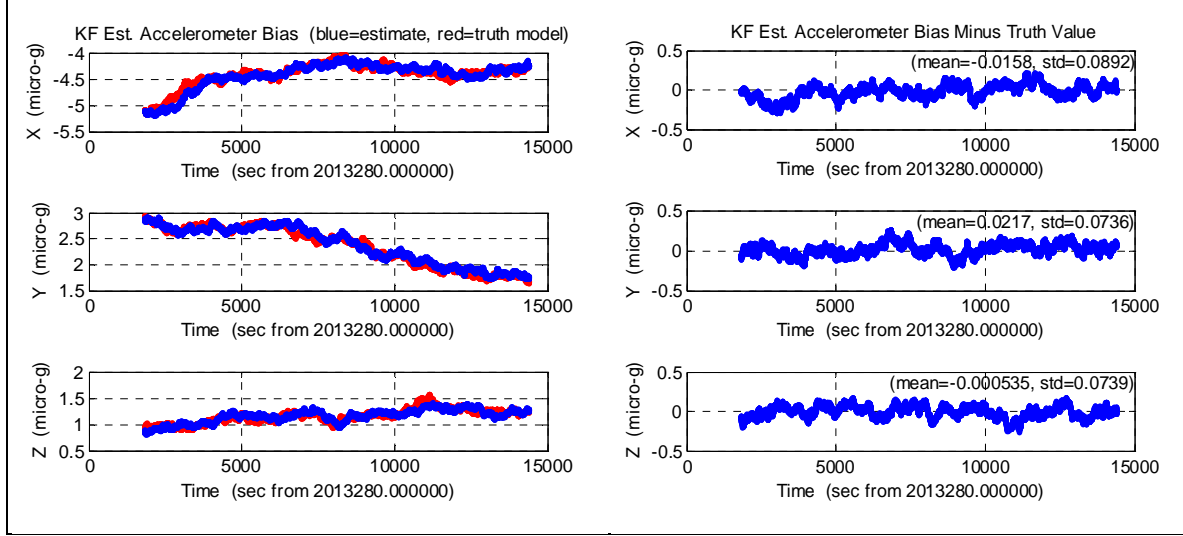


**Fig. 1.** Accelerometer bias estimates (blue) and truth values (red) are shown on the left, and residuals (estimates minus truth) are shown on the right.

The bias filter was also tested using data from a high-fidelity flexible body simulation. This simulation included significant wire boom and appendage vibrations such that the core body underwent oscillations with an amplitude of up to 0.4 deg. There were several characteristic frequencies, but the dominant period was 100 seconds. These tests also included a variety of inertia tensor errors.

As discussed in the next section, errors in the modeled inertia tensor can cause coning angle errors and nutation frequency errors. Coning is caused when the modeled major principal axis of inertia differs from the body Z-axis, and coning error occurs when this principal axis does not agree with that of the truth model. Similarly, nutation frequency error is caused when the modeled ratio of the transverse and axial moments of inertia does not agree with that of the truth model.

With tests having a run time of four hours and a 4 Hz data frequency, it was found that coning errors have a much larger impact on bias estimate accuracy than do nutation errors. However, if the inertia tensor is calibrated prior to the bias estimation, then the bias accuracy can consistently be kept under the  $2 \mu\text{g}$  ( $3\sigma$ ) tolerance, even in the presence of boom oscillations.

#### 2.4. Inertia Tensor Calibration

Due to the dependence of the MMS EKF on the dynamical model for attitude and rate propagation, the accuracy of the transverse components of the estimated rotation rate, and the subsequent accelerometer bias estimates, are very sensitive to errors in the inertia tensor. For this reason, inertia tensor calibration is included in the AGS suite of utilities.

**2.4.1. Major Principal Axis Estimation.** The goal of the first estimation strategy is to improve knowledge of the direction of the major principal axis of inertia in the body frame. The approach uses the high-accuracy ST measurements to estimate the direction of the angular momentum vector in GCI. It is assumed the major principal axis of inertia will be aligned, on average, with the angular momentum. As detailed below, this provides enough information to determine the direction of the major principal axis in the body. The inertia tensor then is rotated to agree with this estimated principal axis, without making any other changes to the inertia. This strategy has been shown to work even when the spacecraft is experiencing coning, nutation, and/or boom oscillations.

First, the attitude history is determined from a set of ST measurements. From this, the direction of the body Z-axis,  $\hat{Z}_I$ , is computed, where the subscript  $I$  here indicates the vector is referenced to an inertial reference frame, and the caret indicates unit vector. The angular momentum direction,  $\hat{L}_I$ , may be found by calculating the vector around which the Z-axis rotates in inertial space. If there is no nutation, then  $\hat{Z}_I$  will rotate around  $\hat{L}_I$  on a circular cone. If there is nutation then the motion will be more complicated as  $\hat{Z}_I$  will rotate around the major principal axis,  $\hat{P}_I$ , which itself will be rotating around  $\hat{L}_I$ . Given enough data and an integral number of nutation periods,  $\hat{L}_I$  may be found in either case by taking the time-average of the motion of  $\hat{Z}_I$ .

Next, this estimate of the angular momentum direction  $\hat{L}_I$  is converted to the body frame using the known attitude history to yield a set of unit vectors,  $\hat{L}_B$ , where the subscript  $B$  here indicates the vector is referenced to the body frame. Then,  $\hat{L}_B$  is averaged over the entire span of nutation periods and re-unitized to obtain  $\bar{L}_B$ , where the overbar indicates the mean value.

If there is no nutation, all the  $\hat{L}_B$  vectors will be parallel (to within the attitude noise) and nearly equal to  $\bar{L}_B$ . If there is nutation,  $\hat{L}_B$  will sweep out an elliptical cone around  $\bar{L}_B$  in the body frame. In either case, the major principal axis in the body frame,  $\hat{P}_B$ , is approximated by  $\bar{L}_B$ .

Finally, the utility computes the direction cosine matrix (DCM) [8] that rotates the a priori major principal axis,  $\hat{P}_B^{prior}$ , into  $\hat{P}_B$ . This DCM is used in a similarity transform on the a priori inertia tensor,  $J^{prior}$ , to yield a new tensor whose major principal axis is the one estimated. That is,

$$\varphi = \cos^{-1}(\hat{P}_B^{prior} \cdot \hat{P}_B), \quad (9)$$

$$\hat{e} = \frac{\hat{P}_B^{prior} \times \hat{P}_B}{|\hat{P}_B^{prior} \times \hat{P}_B|}, \quad (10)$$

$$M = \cos \varphi I_3 + (1 - \cos \varphi) \hat{e} \hat{e}^T - \sin \varphi [\hat{e} \times], \quad (11)$$

$$J^{new} = M^T J^{prior} M, \quad (12)$$

where the caret indicates unit vector and where  $[\hat{e} \times]$  is the skew-symmetric cross-product operator

$$[\hat{e} \times] = \begin{bmatrix} 0 & -e_z & e_y \\ e_z & 0 & -e_x \\ -e_y & e_x & 0 \end{bmatrix}. \quad (13)$$

Performing this estimation does not give any information about the directions of the inertia tensor's two transverse principal axes. By using a minimal rotation,  $M$ , from the a priori major principal axis to  $\hat{P}_B$ , the original directions of the transverse principal axes are affected very little.

The reference attitude for this calibration comes from the EKF solution (although raw ST attitudes could be used). If the EKF is used, there will be some dependence on the a priori inertia tensor. Once a new tensor is obtained from Eq. 12, the filter can be rerun and the process iterated. Convergence has been found to be very rapid; two or three iterations typically are sufficient to determine the principal axis to within less than an arc-second.

A flexible body simulation was used to stress test the Major Principal Axis Estimation algorithm. In this simulation, the actual instantaneous major principal axis varies with time as the wire booms oscillate. Figure 2 shows the angle between the instantaneous and mean major principal axis (the instantaneous axis is moving roughly on a cone about its mean value, with other oscillations superimposed on that motion). Using the mean inertia tensor as a baseline, an attitude solution was estimated using the EKF, and the major principal axis was determined. Then, the mean inertia tensor used by the EKF was corrupted by offsetting the major principal axis from the truth value by various amounts causing coning errors from 0 to 1 deg. The EKF was rerun, and the major principal axis estimation was repeated. Regardless of the corrupting coning error, the estimator determined exactly the same major principal axis in all cases to within machine precision.

The reproducibility of the estimate to machine precision of course should not be taken as the ultimate accuracy of the method. While that accuracy holds for test corruptions in a given specific data set, results will actually vary slightly from data set to data set due to variations in the ST noise, the boom oscillations, and in the true inertia tensor itself. However, due to the averaging steps in the algorithm, the actual accuracy can be expected to be significantly better than the reference attitude accuracy of 0.1 deg.

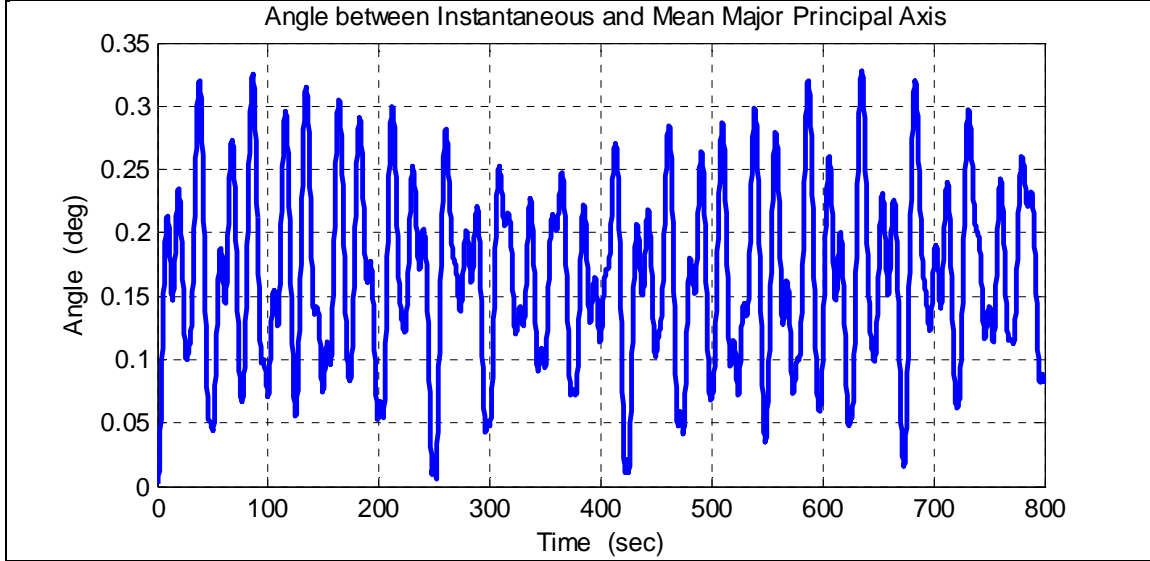


**Fig. 2. Angle between instantaneous and mean major principal axis for inertia tensor calibration test.**

**2.4.2. Inertia Ratio Estimation.** The goal of the second estimation strategy is to improve knowledge of the spacecraft nutation frequency by estimating the ratio of the transverse and axial moments of inertia. This method finds the dominant frequencies in the time-evolution of two geometric parameters. The ratio of these frequencies is simply related to the ratio of the moments of inertia. Before using this algorithm, it is assumed the Major Principal Axis Estimator described above has already been applied to the inertia tensor.

Since it is based on ratios of measured frequencies, the Inertia Ratio Estimation algorithm described here is not expected to work well when flexible modes are significant. For this reason, it is planned to use this part of the inertia calibration utility only prior to deployment of the flexible booms, when the spacecraft can still be considered approximately a rigid body. As such, its value will be in validating the ground-based mechanical model of the inertia tensor for the fully stowed configuration and again after deployment of the rigid magnetometer boom.

For the case of a nutating cylindrical spacecraft, the following relations hold [9]:

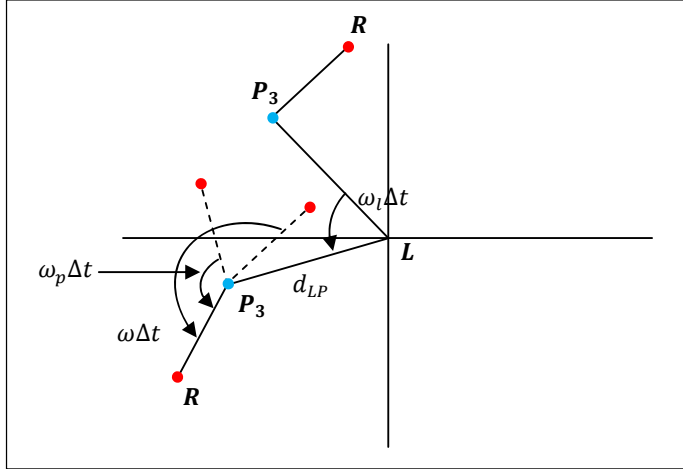
$$\omega^2 = \omega_p^2 + \omega_l^2 + 2\omega_p\omega_l \cos \theta , \quad (14)$$

$$\omega_p = \frac{J_1 - J_3}{J_3} \omega_l \cos \theta , \quad (15)$$

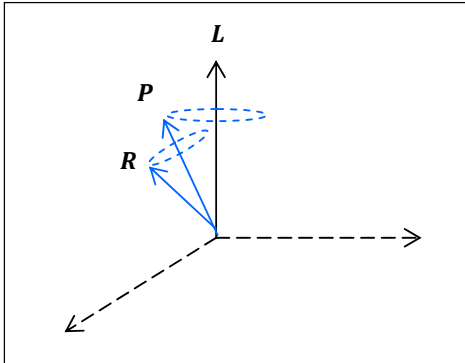
where,  $\omega$  is the instantaneous rotation rate,  $\omega_p$  is the body nutation rate,  $\omega_l$  is the inertial nutation rate,  $J_i$  is the moment of inertia about the  $i$ -th principal axis, and  $\theta$  is the nutation angle. For a non-axisymmetric spacecraft, we use the average of the transverse moments of inertia in place of  $J_1$ .

Figure 3 (based on a diagram in [9]) shows a view looking down onto the plane perpendicular to the angular momentum vector and shows the relationships among the various rates and body vectors as they move in the GCI frame. In this figure, it is assumed the nutation angle is small.

Ultimately, the goal is to correct the inertia tensor based on the ratio in Eq. 15. To do this, it is necessary first to estimate  $\omega_l$  and  $\omega_p$ . By inspection of Fig. 3, it is seen that  $\omega_l$  can be determined by taking the Fourier transform of the X- or Y-component of the major principal axis,  $P_3$ , in an inertial frame perpendicular to the angular momentum vector (that is, in the plane shown in Fig. 3). To estimate  $\omega_p$ , the Fourier transform of the angle between a reference vector  $R$  and the angular momentum vector should be examined. Figure 4 shows this relationship as a 3-dimensional plot where it is clear that this angle's magnitude will oscillate at the body nutation rate,  $\omega_p$ . It is often convenient to take vector  $R$  to be the body Z-axis.



**Fig. 3. Motion in GCI frame of the principal axis  $P_3$  and an arbitrary reference vector  $R$  (constant in the body frame) for a nutating spacecraft. The plot is centered on the angular momentum  $L$ , and  $d_{LP}$  is the projection of  $P_3$  onto the plane perpendicular to  $L$ .**



**Fig. 4. Motion of principal axis  $P$  and arbitrary reference axis  $R$  showing nutation.**

Once  $\omega_l$  and  $\omega_p$  are found, Eq. 15 is used, with the small nutation angle assumption, to calculate  $J_3$ , assuming a constant  $J_1$ . The inertia tensor's largest eigenvalue is then changed to the new  $J_3$ . Note that modifying  $J_3$  and not the transverse moments is an arbitrary choice. The overall scaling of the inertia tensor is not determined by these methods; however, that scaling is only relevant in the presence of external torques and is not needed for improving the nutation modeling.

A set of rigid body simulations was run to test the Inertia Ratio Estimation algorithm. The inertia tensor was corrupted by changing the inertia ratio by 33 percent, causing a large error in the predicted nutation. The EKF used this corrupted inertia tensor to estimate the attitude. Then, the Inertia Ratio Estimation utility used this attitude to compute the parameters described above before Fig. 3. The MATLAB fast Fourier transform (FFT) routine generated the spectra, and the peak frequencies were found, as shown in Fig. 5.

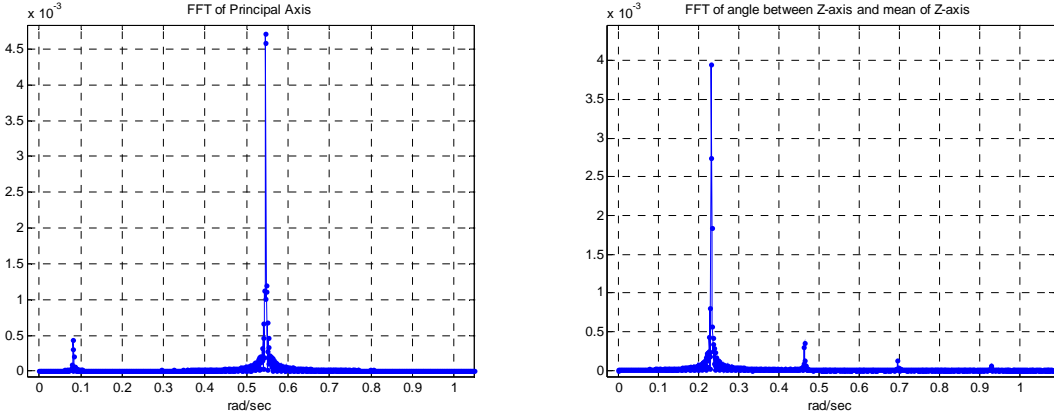


**Fig. 5. Magnitudes (arbitrary units) of FFT of X-component of the major principal axis (left) and FFT of angle between body Z-axis and estimated angular momentum (right).**

The rates  $\omega_l$  and  $\omega_p$  can clearly be identified as the major peaks in the plots shown on the left and right of Fig. 5, respectively. The calibration utility scans these spectra to find the peaks. When Eq. 15 is applied to determine the ratio of the transverse to axial moments of inertia, the error is reduced from 33 percent to 0.046 percent.

As expected, when the calibration utility was tested using a flexible body simulation, it did not yield useful results. Because of the boom oscillations, the FFTs displayed a number of peaks. It was unclear which peaks corresponded to the actual nutation frequencies or whether these nutation frequencies are even well-defined in the flexible body case.

## 2.5. Center of Mass Estimation

During any maneuvers on thrusters, the amount of angular momentum imparted to the space-craft depends on the moment arms of the thrusters relative to the CM. Error in CM knowledge leads to unintended torque and a build-up of angular momentum that then must be unloaded with additional burns. The CM position will be approximately known from engineering designs and ground-based measurements; however, in-flight CM estimation could improve the accuracy of maneuver planning and reduce overall fuel usage.

An algorithm has been designed that estimates the CM using the Doppler shifts of the carrier frequencies from each of the GPS satellites being tracked by the onboard GPS system. Preliminary tests are encouraging, but it is not yet known whether the CM estimates attainable from these Doppler shifts will be accurate enough to be useful. There also are systematic errors that must be considered. These analyses are ongoing and will be reported elsewhere. This section gives a description of the basic algorithm and presents early test results.

Each of the MMS spacecraft is equipped with four GPS receivers (plus four redundant backup receivers) that can simultaneously track up to 12 GPS spacecraft, usually referred to as GPS space vehicles (SVs). These receivers provide data input to the Goddard Enhanced Onboard Navigation System (GEONS) for onboard orbit determination. The AGS will use the GPS carrier frequency Doppler shifts telemetered to the ground from GEONS.

For each SV, the relative motion between it and the MMS spacecraft causes a baseline mean Doppler shift. On top of this will be a very small ripple of the Doppler shift due to the MMS rotational motion that carries the GPS antenna towards and away from the SV. The amplitude of this sinusoidal variation of the Doppler shift is proportional to the projection of the rotational part of the antenna's velocity along the line towards the SV. Thus, fitting the Doppler signal gives us a measurement of that velocity component, which in turn is proportional to the spin rate times the vector from the true CM to the antenna. The difference between this measurement and the prediction based on the nominal CM will be filtered to give the offset of the true CM from its

nominal position. The attitude and all the orbits are known, so the geometric parts of the measurement model are all fully determined except for the CM offset error.

The four GPS antennas are located roughly 1.6 meter from the spin axis and every 90 deg in azimuth. As MMS rotates, the tracked SVs are handed off from one GPS antenna to the next. Thus, there is good observability of the CM in the body  $X$ - $Y$ -plane. However, there is no observability of the CM component along the spin axis. The  $Z$ -component possibly will have some limited observability during orbits after maneuvers when there is significant nutation.

The MMS and GPS SV ephemerides provide the position and velocity vectors of the space-craft CMs in the GCI frame,  $\vec{R}_{MMS}$ ,  $\vec{V}_{MMS}$ ,  $\vec{R}_{GPS}$ , and  $\vec{V}_{GPS}$ . Denote the  $n$ -th GPS antenna location in the MMS body frame as  $\vec{r}_{Ant,n}$ . The nominal CM location in the MMS body frame is  $\vec{r}_{CM0}$ , which is used as the a priori guess for the estimator. The true CM body frame position vector is denoted  $\vec{r}_{CM}$  and its estimate is  $\tilde{\vec{r}}_{CM}$ . The GCI position and velocity of the  $n$ -th antenna are

$$\vec{R}_{Ant,n} = \vec{R}_{MMS} + A^T \Delta \vec{r}, \quad (16)$$

and

$$\vec{V}_{Ant,n} = \vec{V}_{MMS} + A^T \vec{\omega} \times \Delta \vec{r}, \quad (17)$$

where

$$\Delta \vec{r} \equiv \vec{r}_{Ant,n} - \vec{r}_{CM}, \quad (18)$$

and where the transpose of the attitude matrix,  $A^T$ , transforms vectors from the body frame to the GCI frame.

For convenience, define the following body frame and GCI frame vector differences

$$\Delta \vec{R} \equiv A \Delta \vec{R}_I \equiv A(\vec{R}_{GPS} - \vec{R}_{MMS}), \quad (19)$$

and

$$\Delta \vec{V} \equiv A \Delta \vec{V}_I \equiv A(\vec{V}_{GPS} - \vec{V}_{MMS}). \quad (20)$$

Then, the position and velocity of the GPS spacecraft relative to the  $n$ -th antenna, expressed in the body frame, are

$$\vec{R} \equiv A(\vec{R}_{GPS} - \vec{R}_{Ant,n}) = \Delta \vec{R} - \Delta \vec{r}, \quad (21)$$

and

$$\vec{V} \equiv A(\vec{V}_{GPS} - \vec{V}_{Ant,n}) = \Delta \vec{V} - \vec{\omega} \times \Delta \vec{r}. \quad (22)$$

With these definitions, the Doppler shift can be written as

$$f' = \gamma \left( 1 - \frac{\vec{V} \cdot \vec{R}}{c |\vec{R}|} \right) f \quad (23)$$

where  $\gamma = (1 - V^2/c^2)^{-1/2}$ . In the nonrelativistic limit,  $\gamma$  is set to unity and the vector additions in Eqs. 21 and 22 do not make use of the Lorentz transformation. (Further analysis will be done to verify whether this approximation is justified.) The fractional Doppler shift,  $D$ , is defined to be

$$D \equiv \frac{f' - f}{f} = -\frac{\vec{V} \cdot \vec{R}}{c |\vec{R}|}. \quad (24)$$

The quantity  $D$  is the effective measurement for the CM estimator. It must be expanded in  $\Delta \vec{r}$ . Using the notation  $[\vec{\omega} \times]$  for the cross-product operator, defined as in Eq. 13, the inner product in the numerator of Eq. 24 is

$$\begin{aligned} \vec{V} \cdot \vec{R} &= (\Delta \vec{V} - [\vec{\omega} \times] \Delta \vec{r}) \cdot (\Delta \vec{R} - \Delta \vec{r}) \\ &= \Delta \vec{V} \cdot \Delta \vec{R} - ([\vec{\omega} \times] \Delta \vec{r}) \cdot \Delta \vec{R} - \Delta \vec{V} \cdot \Delta \vec{r} + ([\vec{\omega} \times] \Delta \vec{r}) \cdot \Delta \vec{r}. \end{aligned} \quad (25)$$

The denominator of Eq. 24 can be expanded as

$$\begin{aligned} |\vec{R}|^{-1} &= [(\Delta\vec{R} - \Delta\vec{r}) \cdot (\Delta\vec{R} - \Delta\vec{r})]^{-1/2} \\ &\approx [\Delta R^2 - 2\Delta\vec{R} \cdot \Delta\vec{r}]^{-1/2} \\ &\approx \Delta R^{-1} \left[ 1 + \frac{\Delta\vec{R} \cdot \Delta\vec{r}}{\Delta R^2} \right]. \end{aligned} \quad (26)$$

where  $\Delta R$  is the magnitude of  $\Delta\vec{R}$ . The fractional Doppler shift now can be expanded as

$$\begin{aligned} D &\approx \frac{-1}{c\Delta R} [\Delta\vec{V} \cdot \Delta\vec{R} - ([\vec{\omega} \times] \Delta\vec{r}) \cdot \Delta\vec{R} - \Delta\vec{V} \cdot \Delta\vec{r}] \left[ 1 + \frac{\Delta\vec{R} \cdot \Delta\vec{r}}{\Delta R^2} \right] \\ &\approx \frac{-1}{c\Delta R} [\Delta\vec{V} \cdot \Delta\vec{R} - ([\vec{\omega} \times] \Delta\vec{r}) \cdot \Delta\vec{R} - \Delta\vec{V} \cdot \Delta\vec{r} + \Delta\vec{V} \cdot \Delta\hat{R} \Delta\hat{R} \cdot \Delta\vec{r}]. \end{aligned} \quad (27)$$

The sensitivity matrix,  $H$ , is the partial derivative of the observation with respect to the state vector  $\vec{r}_{CM}$ . That is,

$$\begin{aligned} H \equiv \frac{\partial D}{\partial \vec{r}_{CM}} &\approx \frac{-1}{c\Delta R} [\Delta\vec{R}^T [\vec{\omega} \times] + \Delta\vec{V}^T - (\Delta\vec{V} \cdot \Delta\hat{R}) \Delta\hat{R}^T] \\ &= \frac{-1}{c\Delta R} [\Delta\vec{R}_I^T [\vec{\omega}_I \times] + \Delta\vec{V}_I^T - (\Delta\vec{V}_I \cdot \Delta\hat{R}_I) \Delta\hat{R}_I^T] A^T. \end{aligned} \quad (28)$$

Note that one minus sign comes from the partial derivative of Eq. 18,  $\partial\Delta\vec{r}/\partial\vec{r}_{CM} = -I_3$ . The  $H$  matrix is used in a recursive least-squares estimator [9] to determine the value of  $\vec{r}_{CM}$  from a set of  $D$  measurements.

If one is solving for all three components of the CM position, then Eq. 28 gives the appropriate sensitivity matrix. However, the Z-component of the CM has very poor observability due to the  $[\vec{\omega} \times]$  term, and it may be preferred to solve only for the X- and Y-components. In this case, the sensitivity matrix is

$$H_{xy} \equiv \frac{\partial D}{\partial \vec{r}_{CM}} \frac{\partial \vec{r}_{CM}}{\partial (x,y)} = \frac{\partial D}{\partial \vec{r}_{CM}} \begin{bmatrix} 1 & 0 \\ 0 & 1 \\ 0 & 0 \end{bmatrix}. \quad (29)$$

The probable number of GPS SVs that will be tracked by the MMS onboard navigation system varies with orbital position. The number peaks at perigee, and drops rapidly as MMS moves above the GPS constellation. For testing, it was assumed that an average of seven SVs were tracked for six hours centered on the MMS perigee. The data rate was taken to be 1 Hz. (This rate is the same as the onboard single-point GPS solutions, but it is not yet known if this rate will be available in telemetry for AGS use.) The noise on the measured fractional Doppler shift  $D$  was taken to be zero-mean, white, and Gaussian-distributed with a standard deviation of  $10^{-9}$ . The modeled CM offset errors were 4 cm on X and -4 cm on Y. Figure 6 shows a typical result for the X-axis CM estimate under these test conditions (the Y-axis is similar). At the end of the run, the X estimate is 3.51 cm and the Y estimate is -4.10 cm. The test accuracies are consistent with the errors from the estimated covariance matrix, shown as error bounds in Fig. 6.

### 3. Conclusions

The AGS suite of utilities has been prototyped, tested, and shown ready to meet the challenging MMS mission requirements. For its primary attitude and rate estimator, the AGS will use the SpinKF version of the attitude Kalman filter [3]. This filter has been thoroughly tested during support for the ST-5 and THEMIS missions. The AGS will create a daily definitive attitude history using batches of star tracker data with SpinKF. If there are data gaps, these will be interpolated by assuming a constant angular momentum direction and using DSS data to determine the spin phase. This approach has been shown to be feasible to meet the MMS mission requirements for attitude and rate estimation.

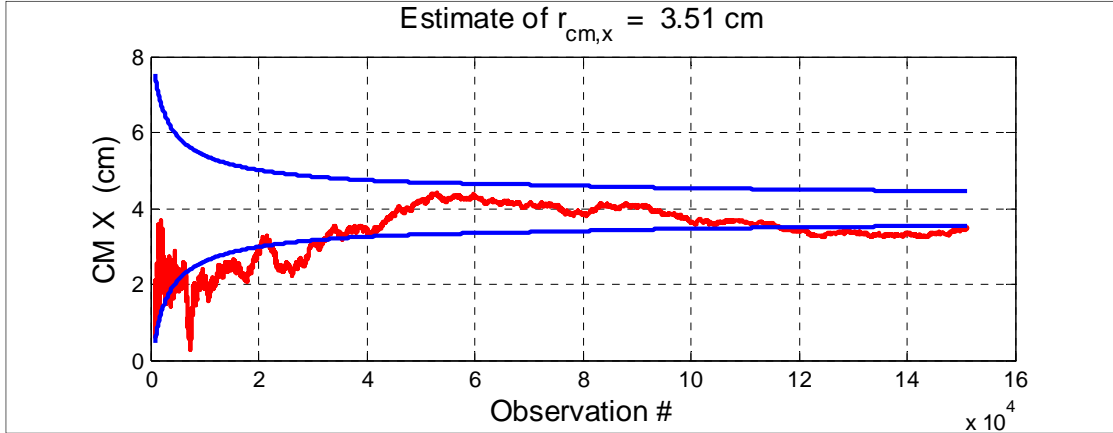


**Fig. 6. Recursive least-squares estimate of X-axis CM offset and  $1\sigma$  error bounds. Truth value is 4 cm.**

The AGS calibration utilities include algorithms for the estimation of sensor alignments, inertia tensor, accelerometer bias, and CM offset. Since the MMS ST has four separate heads, it is convenient to use an attitude-dependent method for estimating the relative alignments [7]. This will be the first AGS calibration performed on-orbit. It may be repeated periodically to ascertain whether seasonal thermal variations affect the alignments, in particular between the two optical benches. The second calibration to be performed will be the inertia tensor estimation. Improved knowledge of the inertia tensor leads to improved rate estimation because the SpinKF must propagate the state between observations using the dynamics equations. Improved rates lead to improved centripetal acceleration prediction (Eqs. 5 and 6), which in turn yields a more accurate accelerometer bias estimation. The bias calibration will be performed prior to every burn to validate the onboard bias estimate.

The AGS team is studying the possibility of estimating the CM on-orbit. This is an important parameter needed for accurate orbit maneuver control. Any error in the CM knowledge leads to errors in the predicted torques during burns, leading to angular momentum build-up. This would necessitate additional thruster firings to unload the excess angular momentum. This paper describes an approach to CM estimation using the raw Doppler shifts of the carrier frequencies from the GPS satellites being tracked by the onboard GPS system. Preliminary results have been very positive although systematic errors have not yet been considered, and the quantity and quality of the available data is still under investigation. As an alternative CM estimation method, the AGS team is actively investigating the possibility of combining accelerometer measurements and onboard GPS point-solutions in either a Kalman filter or a least-squares method.

The AGS suite of utilities has been shown to satisfy the MMS mission requirements, as currently defined. The AGS heritage of use on a wide variety of past missions has demonstrated its capabilities for attitude and calibration support. In addition, the AGS has proven invaluable for attitude-related anomaly resolution on many missions. The new utilities designed for MMS have all been prototyped and have passed preliminary tests. With a robust design and prototypes in hand, the AGS team is ready to move on to formal development and testing and will be ready to support mission rehearsals and launch over the next few years.

#### 4. References

- [1] Shuster, M. D. and Oh, S. D., "Three-Axis Attitude Determination from Vector Observations," *J. Guidance and Control*, Vol. 4, No. 1, Jan.-Feb. 1981, pp. 70-77.
- [2] Langston, J., et al., "A Multimission Three-Axis Stabilized Spacecraft Flight Dynamics Ground Support System," *1992 Flight Mechanics/Estimination Theory Symposium*, NASA Conference Publications CP-3186, NASA/GSFC, Greenbelt, MD, May 1992.

- [3] Markley, F. L. and Sedlak, J. E., "Kalman Filter for Spinning Spacecraft Attitude Estimation," *Journal of Guidance, Control, and Dynamics*, Vol. 31, No. 6, p. 1750, Nov.-Dec. 2008.
- [4] Sedlak, J. E., "Spinning Spacecraft Attitude Estimation Using Markley Variables: Filter Implementation and Results," *2005 Flight Mechanics Symposium*, NASA Conference Publications CP-2005-212789, NASA/GSFC, Greenbelt, MD, Oct. 2005.
- [5] Lefferts, E. J., Markley, F. L., and Shuster, M. D., "Kalman Filtering for Spacecraft Attitude Estimation," *Journal of Guidance, Control, and Dynamics*, Vol. 5, No. 5, pp. 417–429, 1982.
- [6] Markley, F. L., "New Dynamic Variables for Momentum-Bias Spacecraft," *The Journal of the Astronautical Sciences*, Vol. 41, No. 4, pp. 557–567, 1993.
- [7] Hashmall, J. A. and Sedlak, J. E., "New Attitude Sensor Alignment Calibration Algorithms," *53<sup>rd</sup> Int. Astronautical Congress*, IAC-02-A.4.07, IAF, Houston, TX, Oct. 2002.
- [8] Shuster, M. D., "A Survey of Attitude Representations," *Journal of the Astronautical Sciences*, Vol. 41, No. 4, Oct.-Dec., 1993, pp. 439-517.
- [9] Wertz, J. R., (ed.), *Spacecraft Attitude Determination and Control*, D. Reidel Publishing Company, Dordrecht, The Netherlands, 1978.